Theory of Extraordinary Transmission of Light through Quasiperiodic Arrays of Subwavelength Holes

J. Bravo-Abad,[1] A. I. Fernández-Domínguez,[1] F. J. García-Vidal,[1,*] and L. Martín-Moreno[2]
[1]*Departamento de Física Teórica de la Materia Condensada, Universidad Autónoma de Madrid, E-28049 Madrid, Spain*
[2]*Departamento de Física de la Materia Condensada-ICMA, Universidad de Zaragoza, E-50009 Zaragoza, Spain*
(Received 13 June 2007; revised manuscript received 21 August 2007; published 16 November 2007)

By using a theoretical formalism able to work in both real and k spaces, the physical origin of the phenomenon of extraordinary transmission of light through quasiperiodic arrays of holes is revealed. Long-range order present in a quasiperiodic array selects the wave vector(s) of the surface electromagnetic mode(s) that allows an efficient transmission of light through subwavelength holes.

DOI: 10.1103/PhysRevLett.99.203905 PACS numbers: 42.79.Ag, 41.20.Jb, 42.25.Bs, 73.20.Mf

The phenomenon of extraordinary optical transmission (EOT) through periodic two-dimensional (2D) arrays of subwavelength holes milled in a metallic film [1] has sparked a great deal of interest due to both its fundamental implications and its broad range of potential applications. Subsequent experimental and theoretical works have concentrated on analyzing periodic structures [2–10]. However, very recently, several experimental studies showing EOT in quasiperiodic arrays of holes have been reported [11–14]. These results suggest that the presence of long-range order in a 2D hole array is the key ingredient to observe EOT.

In this Letter we present a complete physical explanation of the EOT properties found in quasiperiodic distributions of subwavelength holes. This analysis is based on the comparison between the transmission properties of finite Penrose lattices of holes with those associated with periodic arrays. The picture that emerges from our theoretical study is that the physical origin of EOT is common for both periodic and quasiperiodic arrays. It relies on the excitation of surface electromagnetic (EM) modes decorating the metallic interfaces.

Our study is focused on analyzing the transmission properties of Penrose lattices exhibiting tenfold rotational symmetry, as those studied experimentally in Ref. [14]. As in the experimental structure, the hole radius is chosen to be $a = 0.2$ mm, the thickness of the metallic film is $h = 0.075$ mm and the length of the rhombus side defining the Penrose tiling, d, is $d = 1$ mm. In our simulations, metal is treated as a perfect conductor (i.e. with dielectric constant $\epsilon = -\infty$), which is an excellent approximation in the THz regime. Figure 1 shows the three different types of hole arrangements considered in this work. Left, center, and right panels correspond to a periodic square lattice, a tenfold Penrose lattice and a random distribution of circular holes, respectively. In all three cases, the film thickness, the number of holes ($N = 1506$), their diameter and the size of the external radius are the same. In this way, the density of holes and the area occupied by them are equal in the three structures, allowing a direct comparison between them. The coordinates in the Penrose lattice were generated by the dual generalized method [15,16]. The periodic structure is a circular portion of a square lattice with lattice parameter $P = 0.89$ mm. In the disordered case, N holes are randomly distributed but without allowing any inter-

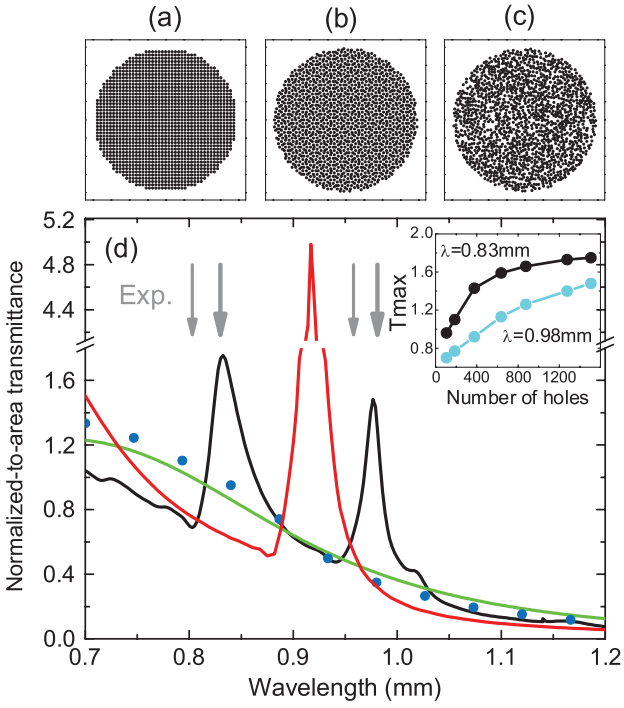

FIG. 1 (color). (a)–(c) Structures considered in this work. Square (left), Penrose (center), and random lattices (right). (d) Normalized-to-area transmittance (T) spectra for single hole (green line), square array (red line), Penrose lattice (black line), and a random configuration (blue dots). In all four cases, $a = 0.2$ mm, $h = 0.075$ mm, and $N = 1506$. Gray arrows mark the locations of the dips (thin lines) and peaks (thick lines) of the experimental transmittance spectrum for the Penrose lattice as reported in Ref. [14]. Inset in panel (d) shows the dependence with N for T at resonant peaks for the quasiperiodic array, $\lambda = 0.83$ mm (black dots) and $\lambda = 0.98$ mm (cyan dots).

hole distance to be smaller than the minimum one found in the quasiperiodic case.

In order to calculate the scattering properties and EM field distributions, we use a formalism based on a modal expansion of the fields, which allows treating efficiently large numbers of indentations, arbitrarily placed in a metal film. Within this framework [7], EM fields in all space can be expressed in terms of the modal amplitudes of the waveguide modes right at the opening and the exit of the different holes ($E_n(\mathbf{R})$ and $E'_n(\mathbf{R})$, respectively, with $\mathbf{R}$ referring to the 2D array locations and n running over the modes inside the holes). These quantities can be obtained by solving a system of linear equations:

$$\begin{aligned} -\epsilon_n E_n(\mathbf{R}) + \sum_{m,\mathbf{R}'} G_{nm}^{\mathbf{R},\mathbf{R}'} E_m(\mathbf{R}') - G_n^V E'_n(\mathbf{R}) &= I_n(\mathbf{R}), \\ -\epsilon_n E'_n(\mathbf{R}) + \sum_{m,\mathbf{R}'} G_{nm}^{\mathbf{R},\mathbf{R}'} E'_m(\mathbf{R}') - G_n^V E_n(\mathbf{R}) &= 0, \end{aligned} \tag{1}$$

where I_n represents the external illumination and the EM interaction between holes is accounted for the propagator $G_{nm}^{\mathbf{R},\mathbf{R}'}$, that couples mode n in a hole located at $\mathbf{R}$ with mode m at $\mathbf{R}'$. The term ϵ_n is related to the bouncing back and forth of EM fields inside the hole and G_n^V couples the input and exit sides of the hole. Detailed expressions for all the magnitudes appearing in Eqs. (1) can be found in Ref. [7]. Once the set $\{E_n(\mathbf{R}), E'_n(\mathbf{R})\}$ is numerically obtained, the transmittance through the structure can be calculated.

Figure 1(d) depicts the normal incidence transmission spectra computed for the three structures, along with the transmittance associated with a single hole (green line). In all cases, the transmittance is normalized to the flux of light impinging on the area occupied by the holes. In the spectral range considered, the single hole transmittance is a smooth decreasing function of the wavelength. In the ordered case (red line), the transmittance spectrum is also smooth, except close to the resonant peak appearing at $\lambda = 0.92$ mm, where the normalized-to-area transmittance (T) is about 5 for the geometrical parameters we are considering. This is the canonical EOT peak, appearing at a resonant wavelength slightly larger than the lattice parameter. As in the experiments, resonant transmission also appears when holes are arranged in a Penrose lattice (black curve in Fig. 1). In this case, maximum transmission values of about 1.5 are obtained at two resonant wavelengths, $\lambda = 0.83$ mm and $\lambda = 0.98$ mm. The agreement between theory and experiment in the spectral locations of these transmission peaks is excellent [see Fig. 1(d)]. On the other hand, blue dots in Fig. 1(d) demonstrate that EOT does not appear for any distribution of holes: the transmission spectrum for the random array does not show any resonant feature. This is just a representative example of disordered arrays; we have generated several random configurations finding always a nonresonant behavior.

The dependence of EOT on lattice structure can be made more apparent by working with the Fourier components of the modal amplitudes, $E_n(\mathbf{q}) = \sum_{\mathbf{R}} \exp(-\imath\mathbf{q}\mathbf{R}) E_n(\mathbf{R})$. By applying a Fourier-transform to the set of linear Eqs. (1), the structure factor of a given set of holes [$S(\mathbf{q}) = \sum_{\mathbf{R}} \exp(-i\mathbf{q}\mathbf{R})$] appears explicitly in the set of equations governing $\{E_n(\mathbf{q}), E'_n(\mathbf{q})\}$:

$$\begin{aligned} [\Sigma_n(\mathbf{q}) - \epsilon_n] E_n(\mathbf{q}) - G_n^V E'_n(\mathbf{q}) &= I_n S(\mathbf{q} - \mathbf{k}_0), \\ [\Sigma'_n(\mathbf{q}) - \epsilon_n] E'_n(\mathbf{q}) - G_n^V E_n(\mathbf{q}) &= 0, \end{aligned} \tag{2}$$

where

$$\Sigma_n^{(\prime)}(\mathbf{q}) E_n^{(\prime)}(\mathbf{q}) = \sum_m \int d\mathbf{k} G_{mn;\mathbf{k}} S(\mathbf{q} - \mathbf{k}) E_m^{(\prime)}(\mathbf{k}) \tag{3}$$

and $\mathbf{k}_0$ is the in-plane component of the incident wave vector. It is worth noticing that the system of Eqs. (2) is also linear and could be solved by discretization of the continuum variable $\mathbf{q}$. The terms $\Sigma_n^{(\prime)}(\mathbf{q}) E_n^{(\prime)}(\mathbf{q})$ now represent the scattering process that couples $E_n^{(\prime)}(\mathbf{q})$ to the continuum $E_m^{(\prime)}(\mathbf{k})$, the momentum difference being provided by the lattice through $S(\mathbf{q} - \mathbf{k})$. The amplitude of the process depends on $G_{mn;\mathbf{k}}$:

$$G_{mn;\mathbf{k}} = \frac{i}{(2\pi)^2} \sum_{\sigma} Y_{\mathbf{k}\sigma} \langle n|\mathbf{k}\sigma\rangle \langle \mathbf{k}\sigma|m\rangle, \tag{4}$$

where the admittance of the plane wave $\mathbf{k}\sigma$, $Y_{\mathbf{k}\sigma}$, is $g/k_z(\mathbf{k})$ for a p-polarized wave and $k_z(\mathbf{k})/g$ for a s-polarized one, with $g = 2\pi/\lambda$. An important property that can be extracted from Eq. (4) is that $G_{mn;\mathbf{k}}$ diverges whenever a p-polarized diffraction wave goes glancing ($k_z = 0$). When dealing with a finite collection of holes, from a numerical point of view, it is more convenient to work with the system of linear equations in real space [Eqs. (1)]. However, physical insight is gained by analyzing its k-space counterpart [Eqs. (2)], as follows. Let us treat first the simpler system of an infinite periodic array of holes and normal incidence radiation. We have checked that for subwavelength holes it is a very good approximation to only consider the least evanescent mode inside the holes (from now on this mode is labeled as $n = 0$). By taking advantage of Bloch's theorem [$E_0(\mathbf{k} + \mathbf{G}_i) = E_0(\mathbf{k})$ and $S(\mathbf{k}) = \sum_{\mathbf{G}_i} \delta(\mathbf{k} - \mathbf{G}_i)$, $\mathbf{G}_i$ being a reciprocal lattice vector], Eqs. (2) for $\mathbf{k} = \mathbf{k}_0 = \mathbf{0}$ transform into two simple equations for $E_0(\mathbf{0})$ and $E'_0(\mathbf{0})$:

$$\begin{aligned} (\Sigma_0 - \epsilon_0) E_0(\mathbf{0}) - G_0^V E'_0(\mathbf{0}) &= I_0, \\ (\Sigma_0 - \epsilon_0) E'_0(\mathbf{0}) - G_0^V E_0(\mathbf{0}) &= 0, \end{aligned} \tag{5}$$

where $\Sigma_0 = \Sigma_0(\mathbf{0}) = \Sigma'_0(\mathbf{0}) = \sum_{\mathbf{G}_i} G_{00;\mathbf{G}_i}$. In Fig. 2, T (panel a) and $|\Sigma_0 - \epsilon_0|$ (panel b) versus wavelength are depicted for an infinite periodic array (magenta line). The geometrical parameters of this array are the same as the periodic one analyzed in Fig. 1. As Σ_0 diverges at $\lambda = P = 0.89$ mm [as a consequence of the divergence of $G_{00;\pm\mathbf{G}_1}$ at this λ, see Eq. (4)], both $E_0(\mathbf{0})$ and $E'_0(\mathbf{0})$ are

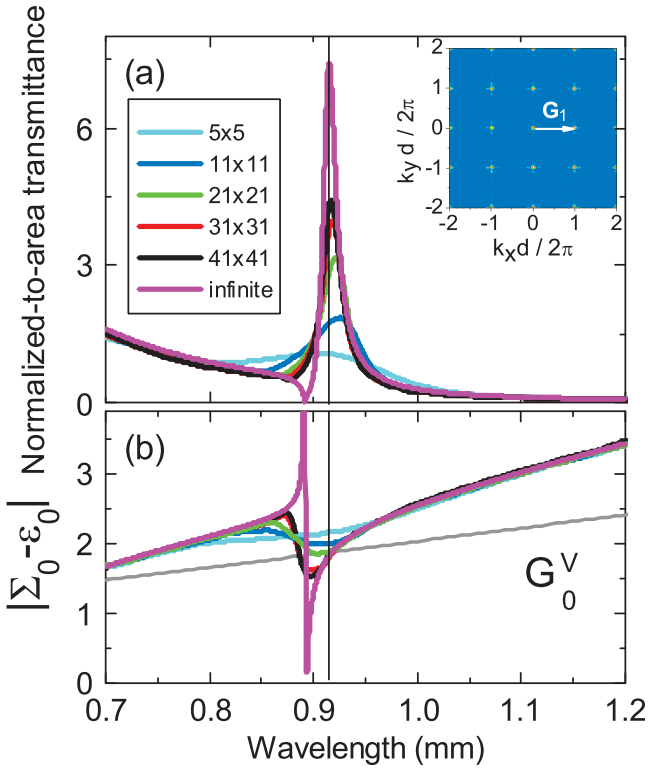

FIG. 2 (color). (a) Normalized-to-area transmittance versus wavelength for an infinite periodic array (magenta line) and several finite square arrays. The geometrical parameters are: $a = 0.2$ mm, $h = 0.075$ mm and $P = 0.89$ mm. Inset shows the structure factor for the 41×41 case. (b) $|\Sigma_0 - \epsilon_0|$ and G_0^V (gray line) versus wavelength for the cases depicted in (a).

zero leading to null transmission. This is the so-called Wood's anomaly [1] or antiresonance as quoted in Ref. [14]. The crucial point to realize is that, due to its rapid variation close to the divergence, at a wavelength slightly larger than the one corresponding to the glancing angle, $|\Sigma_0 - \epsilon_0| = G_0^V$. This leads to a resonant enhancement of the electric field amplitudes at the interfaces of the system [see Eqs. (5)], which can be assigned to the excitation of a leaky surface EM mode [2,17] and, consequently, T presents a maximum at the corresponding wavelength (see Fig. 2).

The arguments presented above can be extended to the case of finite arrays (both periodic and quasiperiodic). Now Bloch's theorem cannot be applied and, in principle, the system of Eqs. (2) must be solved for a continuum of states $\mathbf{q}$. However, we have found that for a finite array with a large number of holes, $\mathbf{q} = \mathbf{k}_0 = \mathbf{0}$ is the dominant transmission channel. Therefore, a good approximation can be obtained by only considering $E_0(\mathbf{0})$ and $E_0'(\mathbf{0})$. The equations for these magnitudes are written like Eqs. (5), where $\Sigma_0 = \Sigma_0^{(l)}(\mathbf{0})$ can be calculated numerically from $E_0^{(l)}(\mathbf{k})$ [see Eq. (3)]. Note that these last quantities can be easily obtained by a Fourier transform of the set of modal amplitudes in real space, $\{E_0(\mathbf{R}), E_0'(\mathbf{R})\}$. Then, within this approach we are able to relate transmission features with properties of just two equations, as in the case of an infinite periodic array. The results of this approach applied to square periodic arrays (going from 5×5 to 41×41) are shown in Fig. 2. Although in finite systems Σ_0 presents no divergences, there is still a resonant feature appearing close to $\lambda = P$. The first consequence is that Wood's anomalies do not reach zero transmittance in finite arrays. As for the infinite case, the cut between $|\Sigma_0 - \epsilon_0|$ and G_0^V marks the location of the transmission peak for large arrays (41×41 and 31×31). For smaller arrays, there is no cut and the transmission peak appears at the wavelength in which the difference between $|\Sigma_0 - \epsilon_0|$ and G_0^V is minimal. We have checked that the approach described above is also valid for quasiperiodic arrays. In panel (b) of Fig. 3, the evolution of $|\Sigma_0 - \epsilon_0|$ versus wavelength is studied for Penrose lattices with increasing number of holes (ranging from $N = 106$ to $N = 1506$, the case analyzed in Fig. 1). $|\Sigma_0 - \epsilon_0|$ present maxima at wavelengths corresponding to the glancing condition for the two main wave vectors of the structure factor [see inset of Fig. 3(a)]: $\vec{b}_1$ ($\lambda_1 = 0.8$ mm) and $\vec{b}_2$ ($\lambda_2 = 0.94$ mm). Consequently, T shows two minima at these two wavelengths. At slightly larger wavelengths, the difference between $|\Sigma_0 - \epsilon_0|$ and G_0^V is minimal and,

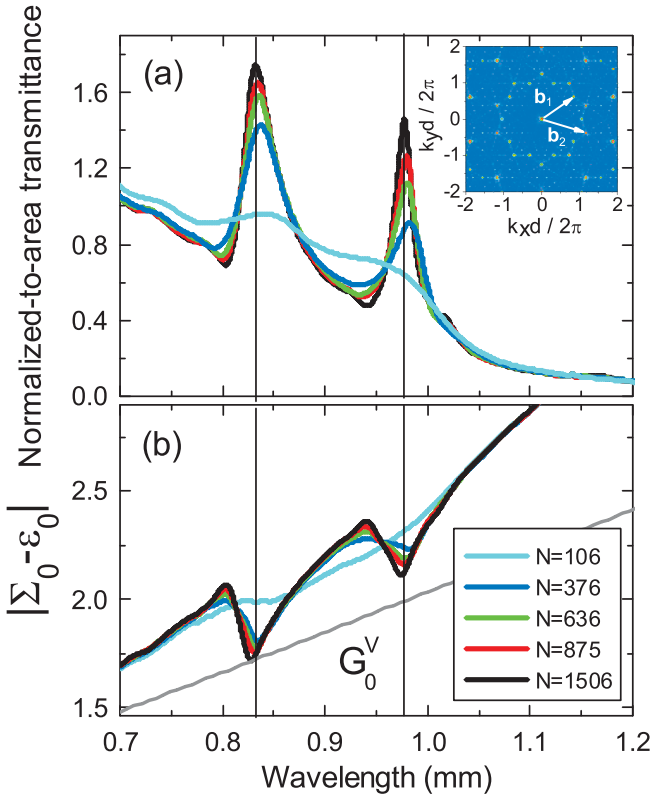

FIG. 3 (color). (a) Normalized-to-area transmittance versus wavelength for several quasiperiodic arrays with different number of holes, N. The geometrical parameters are: $a = 0.2$ mm, $h = 0.075$ mm and $d = 1$ mm. Inset shows the structure factor for the $N = 1506$ case. (b) Both $|\Sigma_0 - \epsilon_0|$ and G_0^V (gray line) versus wavelength for the cases depicted in (a).

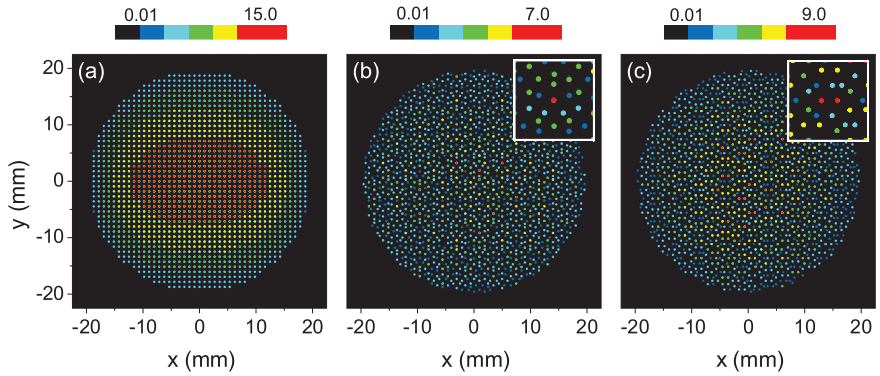

FIG. 4 (color). Transmission per hole (normalized to the single hole transmission) displayed in a color scale for (a) ordered case evaluated at $\lambda = 0.92$ mm, (b) Penrose lattice at $\lambda = 0.83$ mm, and (c) Penrose lattice at $\lambda = 0.98$ mm. Geometrical parameters are the same as in Fig. 1.

correspondingly, two transmission peaks appear in the spectrum. Therefore, these resonant transmission peaks stem from the excitation of surface EM modes at the metallic surfaces, much in the same way as in periodic arrays. Notice that, however, in the quasiperiodic case, there is no minimum wave vector for diffraction [i.e., the structure factor is nonzero for wave vectors with modula smaller than $|\vec{b}_1|$, see inset of Fig. 3(a)]. This results in diffraction onto additional propagating modes in vacuum (other than the zero-order mode), which leads to both smaller resonant peaks and less pronounced Wood's anomalies than those emerging in the periodic case.

It is worth analyzing the spatial distribution of light emerging from the quasiperiodic array. Figure 4 renders the transmission per hole in a Penrose lattice of $N = 1506$ holes at the two resonant wavelengths [$\lambda = 0.83$ mm and $\lambda = 0.98$ mm in panels (b) and (c) of Fig. 4, respectively]. For comparison, panel (a) of Fig. 4 shows the corresponding distribution for the ordered array at the resonant wavelength 0.92 mm. In all three cases, incident **E**-field is pointing along the x direction. In the ordered case, due to finite size effects, the maximum transmission is located at the center of the structure [18]. In quasiperiodic arrangements, the transmission-per-hole distribution presents a completely different pattern: it is far from being uniform, showing the appearance of some holes with high transmission (*hot spots*), which are highlighted in the insets of panels (b) and (c). Interestingly, in the Penrose lattice, for a given resonant wavelength, hot spots show similar local environment. However, the existence of hot spots does not imply that EOT in quasiperiodic systems is dominated by very localized resonant configurations of holes. Calculations (not shown here) on finite clusters of holes centered at the hot spots show an increase of transmittance as a function of the number of neighbors included in the cluster. This point is reinforced by the fact that the resonant peaks observed in the transmission spectra of finite Penrose lattices do not saturate for small N values [see inset of Fig. 1(d)]. Both these results are consistent with the interpretation based on extended leaky surface EM modes described above.

In conclusion, by developing a k-space theoretical formalism, we have been able to demonstrate that the resonant features observed in the transmission spectra of 2D Penrose lattices of holes can be explained in terms of the formation of surface EM modes at the interfaces of the metal film. Furthermore, we have linked the formation of these modes to the structure factor of the hole arrays, enabling the understanding of the appearance of extraordinary optical transmission in more general conditions.

Financial support by the Spanish MECD under Grant No. BES-2003-0374 and Contract No. MAT2005-06608-C02 is gratefully acknowledged.

*Corresponding author.
fj.garcia@uam.es

[1] T. W. Ebbesen *et al.*, Nature (London) **391**, 667 (1998).
[2] L. Martin-Moreno *et al.*, Phys. Rev. Lett. **86**, 1114 (2001).
[3] J. Gomez Rivas *et al.*, Phys. Rev. B **68**, 201306(R) (2003).
[4] R. Gordon *et al.*, Phys. Rev. Lett. **92**, 037401 (2004).
[5] W. L. Barnes *et al.*, Phys. Rev. Lett. **92**, 107401 (2004).
[6] K. J. Klein Koerkamp *et al.*, Phys. Rev. Lett. **92**, 183901 (2004).
[7] J. Bravo-Abad, F. J. García-Vidal, and L. Martín-Moreno, Phys. Rev. Lett. **93**, 227401 (2004).
[8] J. T. Shen, P. B. Catrysse, and S. Fan, Phys. Rev. Lett. **94**, 197401 (2005).
[9] P. Lalanne, J. C. Rodier, and J. P. Hugonin, J. Opt. A Pure Appl. Opt. **7**, 422 (2005).
[10] A. P. Hibbins *et al.*, Phys. Rev. Lett. **96**, 073904 (2006).
[11] M. Sun *et al.*, Chin. Phys. Lett. **23**, 486 (2006).
[12] A. S. Schwanecke *et al.*, OSA Nanophotonics Topical Meeting, April 2006 (to be published).
[13] F. Przybilla, C. Genet, and T. W. Ebbesen, Appl. Phys. Lett. **89**, 121115 (2006).
[14] T. Matsui *et al.*, Nature (London) **446**, 517 (2007).
[15] D. Levine and P. J. Steinhardt, Phys. Rev. B **34**, 596 (1986).
[16] D. A. Rabson, N. D. Mermin, D. S. Rokshar, and D. C. Wright, Rev. Mod. Phys. **63**, 699 (1991).
[17] J. B. Pendry, L. Martín-Moreno, and F. J. García-Vidal, Science **305**, 847 (2004).
[18] J. Bravo-Abad *et al.*, Nature Phys. **2**, 120 (2006).